Journal of
Materials Chemistry B

Materials for biology and medicine

Accepted Manuscript

This article can be cited before page numbers have been issued, to do this please use: Y. Gu, X. Bi and J. Ye, *J. Mater. Chem. B*, 2020, DOI: 10.1039/D0TB00659A.

ROYAL SOCIETY OF CHEMISTRY

rsc.li/materials-b

View Article Online
DOI: 10.1039/D0TB00659A

Gap-enhanced Resonance Raman Tags for Live-Cell Imaging

Yuqing Gu,[†,‡] Xinyuan Bi,[‡] and Jian Ye[,†,‡,#]*

[†]Department of Nuclear Medicine, Ruijin Hospital, School of Medicine, Shanghai Jiao Tong University, Shanghai 200025, P.R. China

[‡]State Key Laboratory of Oncogenes and Related Genes, School of Biomedical Engineering, Shanghai Jiao Tong University, Shanghai, P. R. China

[#]Shanghai Key Laboratory of Gynecologic Oncology, Ren Ji Hospital, School of Medicine, Shanghai Jiao Tong University, Shanghai, P. R. China

RECEIVED DATE (to be automatically inserted after your manuscript is accepted if required according to the journal that you are submitting your paper to)

[*]To whom correspondence should be addressed. E-mail: yejian78@sjtu.edu.cn

View Article Online
DOI: 10.1039/D0TB00659A

Abstract

Surface-enhanced Raman scattering (SERS) nanotags are widely used in biomedical field including live-cell imaging due to the high specificity from their fingerprint spectrum and the multiplexing capability from the ultra-narrow linewidth. However, long-term live-cell Raman imaging is limited due to the photodamage from a relatively long exposure time and a high laser power, which are needed for acquiring detectable Raman signals. In this work, we attempt to resolve this issue by developing ultrabright gap-enhanced resonance Raman tags (GERRTs), consisting of the petal-like gold core and silver shell with near-infrared resonant reporters of IR-780 embedded in between, for long-term and high-speed live-cell imaging. GERRTs exhibit the ultrahigh Raman intensity down to a single-nanoparticle level in the aqueous solution and solid state upon 785 nm excitation, allowing for high-resolution time-lapse live-cell Raman imaging with an exposure time of 1 ms per pixel and a laser power of 50 μW. Under this measurement condition, we can possibly capture dynamic cellular processes with a high temporal resolution, and track living cells for long periods of time owing to the reduced photodamage to cells. These nanotags open new opportunities for ultrasensitive, low-phototoxic, and long-term live-cell imaging.

Keywords: surface-enhanced Raman scattering (SERS), gap-enhanced resonance Raman tags (GERRTs), single-nanoparticle detection, live-cell imaging, long-term tracking

View Article Online
DOI: 10.1039/D0TB00659A

TOC

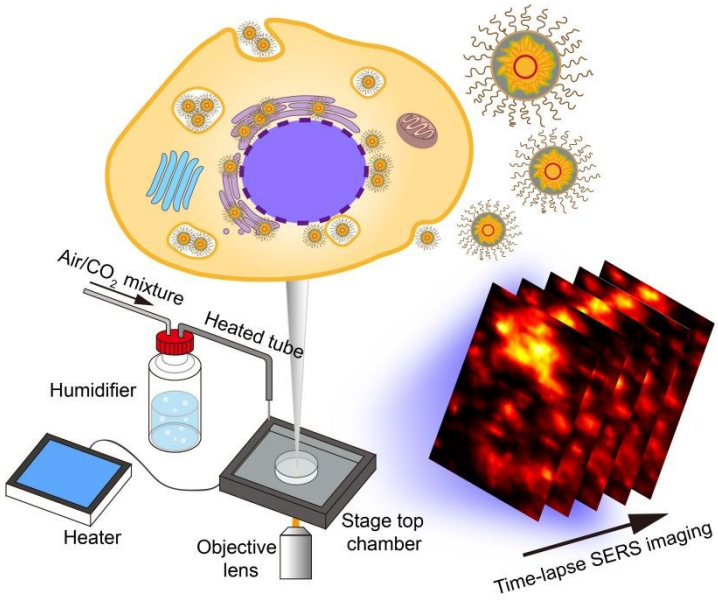

Gap-enhanced resonance Raman tags enable long-term, high-resolution and high-speed (1 ms/pixel) live-cell imaging with a laser power of 50 μW.

View Article Online
DOI: 10.1039/D0TB00659A

Introduction

Surface-enhanced Raman scattering (SERS) has been substantially used as an analytical technique in many scientific fields.[1-4] SERS tags based on plasmonic nanostructures have attracted great interest in biomedical applications such as biomolecule detection,[5,6] circulating tumor cell detection,[7] cellular microenvironment sensing,[8] and cell/tissue imaging[9-11] owing to the advantageous high specificity, sensitivity and noninvasion. Compared to fluorophores, SERS tags usually exhibit advantages including better photostability,[12] larger multiplexing capability due to their narrower spectral linewidth, and avoidance of the autofluorescence from biological samples with near-infrared (NIR) excitation. SERS spectroscopy has been applied as an analytical tool in live cells to monitor cellular local pH,[13] probe biomolecules[14,15] or cell secretions,[16] follow the kinetics of drug delivery,[17] study the dynamics of physiological processes,[18,19] and track cellular uptake pathways of nanoparticles (NPs).[20] Unlike imaging for fixed cells, we should control the measurement parameters including exposure time and laser power to minimize the photodamage to live cells. For example, Kang et al. has demonstrated high-resolution live cell SERS imaging with an exposure time of 10 ms per pixel and 200 μW laser power.[21] However, we believe that the photodamage can be further alleviated by increasing the brightness of SERS tags, which is of great significance for long-term live cellular tracking. In addition, the imaging speed can be further improved with shortened acquisition time, allowing to record dynamic processes of cells with a high temporal resolution.

Surface-enhanced resonance Raman scattering (SERRS) NPs have been developed in recent years as ultrasensitive tags.[22-24] It has been widely accepted that the SERS phenomenon is mainly attributed to electromagnetic (EM) enhancement and chemical enhancement (CE). The former arises from the “hot

View Article Online
DOI: 10.1039/D0TB00659A

spots" generated by the surface plasmon resonance (SPR) of plasmonic nanostructures,[25] which contributes to the signal enhancement by 10^6 - 10^9.[26] The latter originates from the interaction between chemisorbed molecules and the metal surface,[25] which provides 10 to 10^3 fold of enhancement to the Raman intensity.[27] In addition, SERRS effect occurs when the optical absorption of reporter molecules overlaps with the excitation laser wavelength, further increasing the Raman intensity by two to three orders of the magnitude.[28] SERRS tags has been demonstrated with great potentials in ultrasensitive biomedical imaging with an attomolar detection limit.[24] For instance, Kircher et al. have realized high-precision cancer imaging[22] and lymph node metastases detection[29] with SERRS probes at low injection doses.

When the Raman reporters are physiosorbed onto gold (Au) or silver (Ag) NPs, a protective layer is usually required to prevent the leakage of reporters. Typical plasmonic NPs (e.g., nanospheres and nanorods) with a protection layer like silica,[30] polydopamine[31] or bovine serum albumin[32] can only offer moderate Raman enhancement. In recent years, there has been increasing interest in designing a new type of SERS tags where the Raman reporters are embedded between the metallic core and shell,[30,33-36] also called gap-enhanced Raman tags (GERTs).[9,12,37] The shell can protect the embedded molecules from desorption and degradation,[35] and the plasmon coupling between core and shell can provide large and uniform EM field,[9,35,38] resulting in stable, reproducible and ultra-strong Raman signals;[9,35,36] meanwhile, GERTs exhibit improved photostability compared with conventional SERS tags.[12,39] Therefore, GERTs hold great promise in bioimaging applications.[10,11,40] For example, we have recently reported[9] Au GERTs with a petal-like shell structure (P-GERTs for brevity), showing an ultrahigh sensitivity down to a single-NP level and allowing high-resolution single cell imaging with an exposure time of ~1 ms per pixel and a laser power of 370 μW.[9]

View Article Online
DOI: 10.1039/D0TB00659A

In this work, we have developed a new type of ultrasensitive core-shell SERRS tags, termed gap-enhanced resonance Raman tags (GERRTs), for long-term and high-speed live-cell bioimaging. The GERRTs consist of the aforementioned P-GERT as the core and a Ag shell with Raman reporters of IR-780, a dye resonant in NIR window, embedded in between. Utilizing a great amount of strong EM hot spots from the petal-like shell structure and large immobilization surface area of P-GERTs as well as the SERRS effect of NIR-resonant IR-780, GERRTs show three orders of magnitude stronger Raman signals than P-GERTs and a detection sensitivity down to a single-NP level in the aqueous solution and solid state. Additional surface modifications of polydopamine (PDA) and polyethylene glycol (PEG) improve the biocompatibility of GERRTs, therefore allowing for high-speed and high-resolution live cell imaging (2500 pixels) can be acquired within 12 s with an exposure time of 1 ms per pixel and a laser power of 50 μW. Such a short frame acquisition time enables to possibly capture the dynamic processes of live cells with a high temporal resolution. In addition, we expect that the photodamage to living cells can be significantly reduced under above-mentioned measurement parameters, hence allowing the long-term survival of cells and time-lapse Raman imaging of live Hela cells for up to 8 h with the aid of the integrated air-tight live-cell incubation system.

Experimental section

Materials. IR-780 iodide (98%), tris(hydroxymethyl)aminomethane (Tris, ≥ 99.8%) and hydrochloric acid (HCl, 37 wt.%) were acquired from Sigma-Aldrich (Shanghai, China). Chloroauric chloride ($HAuCl_4 \cdot 4H_2O$) and N,N-dimethylformamidel (DMF, ≥ 99.0%) were received from Sinopharm Chemical Reagent Co. Ltd (Shanghai, China). 4-Nitrobenzenethiol (4-NBT, 90%) was obtained from Fluorochem Ltd

View Article Online
DOI: 10.1039/D0TB00659A

(Derbyshire, United Kingdom). Cetyltrimethylammonium chloride (CTAC, 99%) and dopamine hydrochloride (98%) were purchased from J&K Chemical Ltd (China). Silver nitrate ($AgNO_3$, 99.8%), ascorbic acid (AA, > 99.0%) and thiol PEG acid (HS-PEG-COOH, MW = 5000 Da) were obtained from Aladdin (China). All materials were used as received without any further purification. Ultrapure water (18.2 MΩ) was used for all experiments.

Synthesis of GERRTs. P-GERTs were synthesized according to our previous work.[9] Briefly, 100 μL 4-NBT ethanol solution (10 mM) was added to 2 mL 22 nm Au cores[36] under vigorous sonication followed by the incubation at 25 °C for 5 min. The 4-NBT modified Au cores were then washed with CTAC (50 mM) three times and resuspended in 50 mM CTAC solution. Finally, P-GERTs were obtained by adding 480 μL AA (40 mM) and 960 μL reporter-modified core solution in turn into the mixture of 16 mL CTAC (50 mM) and 800 μL $HAuCl_4$ (4.86 mM) under vigorous sonication. For the synthesis of GERRTs, 200 μL DMF solution of IR-780 iodide (0.16 mM) was added dropwise to 1 mL P-GERTs (0.06 nM) under ultra-sonication, followed by 1 h incubation in 32 °C water bath. Next, 1.2 mL dye-modified P-GERTs were added to a mixture of 2.5 mL CTAC (25 mM), 400 μL $AgNO_3$ (14.58 mM) and 1.875 mL AA (40 mM). The mixture was then incubated in 70 °C water bath for 3 h. Finally, the obtained GERRTs were washed with CTAC (100 mM) twice to remove excess IR-780 molecules and redispersed in water.

Surface functionalization. The polymer surface coating was applied to GERRTs in accordance with Zhang's protocol with some modifications.[41] For polydopamine coating, 12 mL GERRTs (0.01 nM) was mixed with 12 mL dopamine hydrochloride solution (0.01 mg/mL) buffered to pH = 8.5 using 10 mM Tris solution. The mixture was sonicated for 20 min and then centrifuged once followed by redispersion in 400 μL water. For PEG modification, the redispersed NPs were dissolved in 800 μL aqueous HS-PEG-

View Article Online
DOI: 10.1039/D0TB00659A

COOH (10 mg/mL) and vortexed for 2 min. The mixture was kept at 4 °C overnight and then GERRTs@PDA@PEG were harvested by centrifugation and washed with pure water twice.

Characterizations of NPs. Transmission electron microscope (TEM) images were collected on a JEM-2100F transmission electron microscope (JEOL, Tokyo, Japan) operated at 200 kV. High-angle annular dark-field scanning TEM (HAADF-STEM) and energy dispersive X-ray (EDX) mapping analyses were performed on a TALOS F200X transmission electron microscope (200 kV, FEI, USA) equipped with an EDX system with four SDD probes. UV-Vis extinction spectra were measured from a UV1900 UV-vis spectrophotometer (Aucybest, Shanghai, China). Raman measurements and cell imaging were carried out on an inverted confocal Raman microscope with 785 nm laser (Xplora INV, Horiba). Single NP analyses were performed on a correlative Raman imaging and scanning electron microscopy (RISE, TESCAN, Czech). Dynamic light scattering (DLS) and zeta potential measurements were performed on a Zetasizer Nano ZSP (Malvern, UK).

The detection limit of aqueous GERRTs. The detection limit of aqueous GERRTs was determined by conducting Raman measurements on GERRT solutions at various concentrations from 10^{-11} to 10^{-16} M with ×10 objective lens (NA = 0.3), 29.8 mW laser power and 10 s acquisition time. 100 SERS spectra were collected for each concentration of homogenous GERRT solution for data analysis.

Raman measurements of single GERRTs on RISE. The integrated RISE system was applied for single-GERRT detection after the aqueous sample (1 pM) was air-dried on a silicon wafer with some metallic marks for easier location. To avoid the damage of electron beam to NPs and Raman reporters, the monodispersed single GERRTs were first identified under the bright field. Raman signals were collected from the NPs using 785 nm laser, ×100 objective lens, 1 mW laser power and 20 s acquisition time. Then, the sample was automatically transferred to the SEM chamber to confirm the distribution states of the

View Article Online
DOI: 10.1039/D0TB00659A

measured NPs. The data only from single GERRTs with a distance of more than 1 μm from other NPs were analyzed.

Cell culture. The Hela cell line was purchased from Cell Library of the Chinese Academy of Sciences (Shanghai, China), and all reagents for cell culture were obtained from Gibco. The cells were cultured in a Dulbecco's modified Eagle's medium (DMEM) with 10% fetal bovine serum (FBS), 100 μg/mL penicillin and 100 μg/mL streptomycin in a water-jacketed incubator at 37 °C with 5% CO_2-humidified atmosphere.

Cell cytotoxicity evaluation. The cytotoxicity of GERRTs@PDA@PEG was evaluated using Hela cells through CCK-8 assay (Cell Counting Kit-8, Dojindo). Hela cells were seeded in 96-well plates at a density of 4×10^3 cells per well, and cultured in DMEM at 37 °C in a humidified atmosphere containing 5% CO2. After 24 h, the culture medium was replaced by fresh DMEM with different concentrations of 0, 0.002, 0.01, 0.05, 0.1 and 0.2 nM. Each concentration was set at least six parallel wells. Then, the cells were cultured for another 24 h. After that, the culture medium was refreshed with new DMEM containing 10% CCK-8, and the CCK-8-contained medium was added to another six empty wells as background. After 2 h incubation, the absorbance was measured spectrophotometrically using an enzyme-linked immunosorbent assay microplate reader (Synergy 2, Bio-TEK).

Live-cell imaging. Hela cells were firstly cultured in a quartz dish and allowed to adhere to the dish bottom for 24 h. Then, the culture medium was replaced by new DMEM with GERRTs@PDA@PEG at a final concentration of 0.05 nM. The dish was immediately placed in UNO STAGE TOP INCUBATOR (Okolab, Italy) set at 37 °C with 5% CO_2-humidified atmosphere. The live-cell incubation system is integrated with the inverted confocal Raman microscope with an airtight chamber. Time-lapse Raman imaging of live Hela cells was conducted at different time points with 785 nm laser, ×60 objective lens

View Article Online
DOI: 10.1039/D0TB00659A

and 1 ms acquisition time using Duoscan/SWIFT mode.[9] Cell culture in the chamber lasted for about 24 h.

Results and discussion

Preparation and characterization and GERRTs. Bimetallic GERRTs were synthesized through a wet-chemical metal-ion-reduction method to form multiple metallic shells on Au cores, as presented in Figure 1A. First, uniform-sized Au cores[36] (Figure 1A i) were modified with a monolayer of 4-NBT molecules, which link covalently to Au surface via the thiol group. Next, the molecule-modified Au cores (Figure 1A ii) were utilized as seeds to grow the outer Au shell, thus obtaining GERTs with a petal-like shell structure (P-GERTs, Figure 1A iii), which can be confirmed by the TEM image in Figure 1B iii. 4-NBT molecules were selected because of a large Raman cross-section and the poor affinity between Au shell and its nitro group, resulting in the formation of a number of small Au nuclei on cores and the consequent petal-like shell structure.[9] After that, the Raman reporter IR-780 was allowed to adsorb to CTAC-stabilized P-GERTs through hydrophobic interaction between IR-780 and CTAC.[42] Herein, P-GERTs have been selected as templates owing to a large quantity of immobilization sites and SERS "hot spots" for reporter molecules provided by the large surface area and multiple nanogaps of petal-like shells, therefore leading to a strong Raman enhancement.[9] IR-780, a NIR resonant dye, has a pronounced absorption peak at 780 nm (Figure 1D), which matches well with the excitation laser wavelength 785 nm, and therefore can produce SERRS effect. Finally, a Ag layer of coating was applied to IR-780 modified P-GERTs to achieve spherical GERRTs (Figure 1A v). The Ag shell serves as a protective layer to prevent

View Article Online
DOI: 10.1039/D0TB00659A

the leakage of physically-adsorbing IR-780 molecules. Meanwhile, we can take advantage of the high SERS activity of Ag to further increase the Raman intensity of GERRTs.

TEM examinations of the NPs at different synthesis stages show that their diameters are around 22, 66 and 130 nm for Au cores, P-GERTs and GERRTs, respectively, all with a monodispersed particle size and the uniform morphology (Figure 1B and Figure S1). P-GERTs have a uniform interior nanogap between the core and shell (indicated by red arrows in Fig. 1B iii) with a typical size of below 1 nm,[9,43] which is determined by the molecular length of 4-NBT molecule and its orientation angle on Au cores.[43] We can only roughly distinguish the outer Ag shell and the internal darker Au P-GERT via the image contrast from the high-resolution TEM image of GERRTs (Figure 1B v). Therefore, we further performed STEM and EDS characterizations to have a better view of the structure and element distribution of GERRTs, as shown in Figure 1C. The petal-like GERTs inside the Ag shell and even the interior nanogap can be clearly observed from the STEM image. Meanwhile, the corresponding element distributions (Au, Ag) coincide well with the STEM image, further confirming the Au-Ag core-shell structure of GERRTs. The Au cores present a ruby color with a single localized surface plasmon resonance (LSPR) peak at 529.2 nm (Figure 1D i), and a gentle redshift of 2.1 nm after 4-NBT modification due to the slight change of the reflective index (Figure 1D ii).[44] P-GERTs exhibit a dark blue color with a pronounced redshift of the LSPR peak at 594 nm with a relatively broad linewidth due to the strong plasmon coupling of petal-like shell structure. In contrast, GERRTs show a light-yellow color with two pronounced LSPR peaks at 439 and 566 nm. The former is attributed to the Ag shell coating and the latter is due to the blue-shifted plasmon band of internal P-GERTs. The changes in extinction spectra comply with the previously reported work[45] and can further confirm the successful coating of the Ag layer.[16]

View Article Online
DOI: 10.1039/D0TB00659A

We then turn to investigate the SERS performance of GERRTs, as presented in Figure 1E. It can be observed that the SERS spectrum of GERRTs upon 785 nm excitation exhibits many characteristic bands, with four main bands of out-of-plane substituent sensitive vibration of phenyl ring[46] at 523 cm^{-1}, in-plane deformation of phenyl ring[46] at 557 cm^{-1}, C-H in-plane deformation[47] at 1206 cm^{-1} and Fermi resonance interaction of the indole ring N1C8 stretching vibration combined with out-of-plane bending vibrations[48] at 1369 cm^{-1}. While P-GERTs exhibit one relatively strong Raman band at 1338 cm^{-1} from ν (NO_2) mode of 4-NBT molecules (Figure 1E iii and Figure S2).[9] We have previously reported the ultrahigh Raman intensity of P-GERTs due to the multiple hot spots with an enhancement factor beyond 1×10^9,[9] but it should be noted that the Raman enhancement of GERRTs can be further greatly improved. For example, the intensity of GERRTs becomes saturated under the same measurement condition as P-GERTs we used before in Figure S2.[9] After normalization, we can estimate that the Raman intensity of GERRTs is more than three orders of magnitude higher than that of P-GERTs by comparing the Raman band at 1206 cm^{-1} for the former and 1338 cm^{-1} for the latter (see Figure 1E). We presume that such strong Raman signals of GERRTs can be attributed to several factors. First, a large number of hot spots provided by petal-like shells along with the plasmon coupling between Au and Ag layer can generate strong electromagnetic enhancement for IR-780. Second, the resonance of the optical absorption of IR-780 with the excitation laser can produce resonant Raman scattering, further increasing the Raman intensity. Third, the iodide ion in IR-780 may also possibly contribute to the ultrahigh Raman signal, since it has been reported that halide ions (Cl^-, Br^- and I^-) have a substantial activating effect in chemical enhancement.[49] We further conducted concentration-dependent Raman measurements to challenge the sensitivity of GERRTs. Figure 1F shows the representative SERS spectra acquired from aqueous GERRTs with various concentrations from 1 pM to 1 fM, indicating clear observation of the characteristic band of IR-780 at 1206 cm^{-1} even at the lowest

View Article Online
DOI: 10.1039/D0TB00659A

concentration of 1 fM (Figure S3). In addition, we find that Raman signals of GERRTs can be constantly detected at concentrations of 1 pM, 100 fM and 10 fM, but only signals in around a quarter of measurements at the concentration of 1 fM, and no signals down to 0.1 fM (Fig. S3 and S4), which is reaching a single-NP level according to the Kneipp's method.[50]

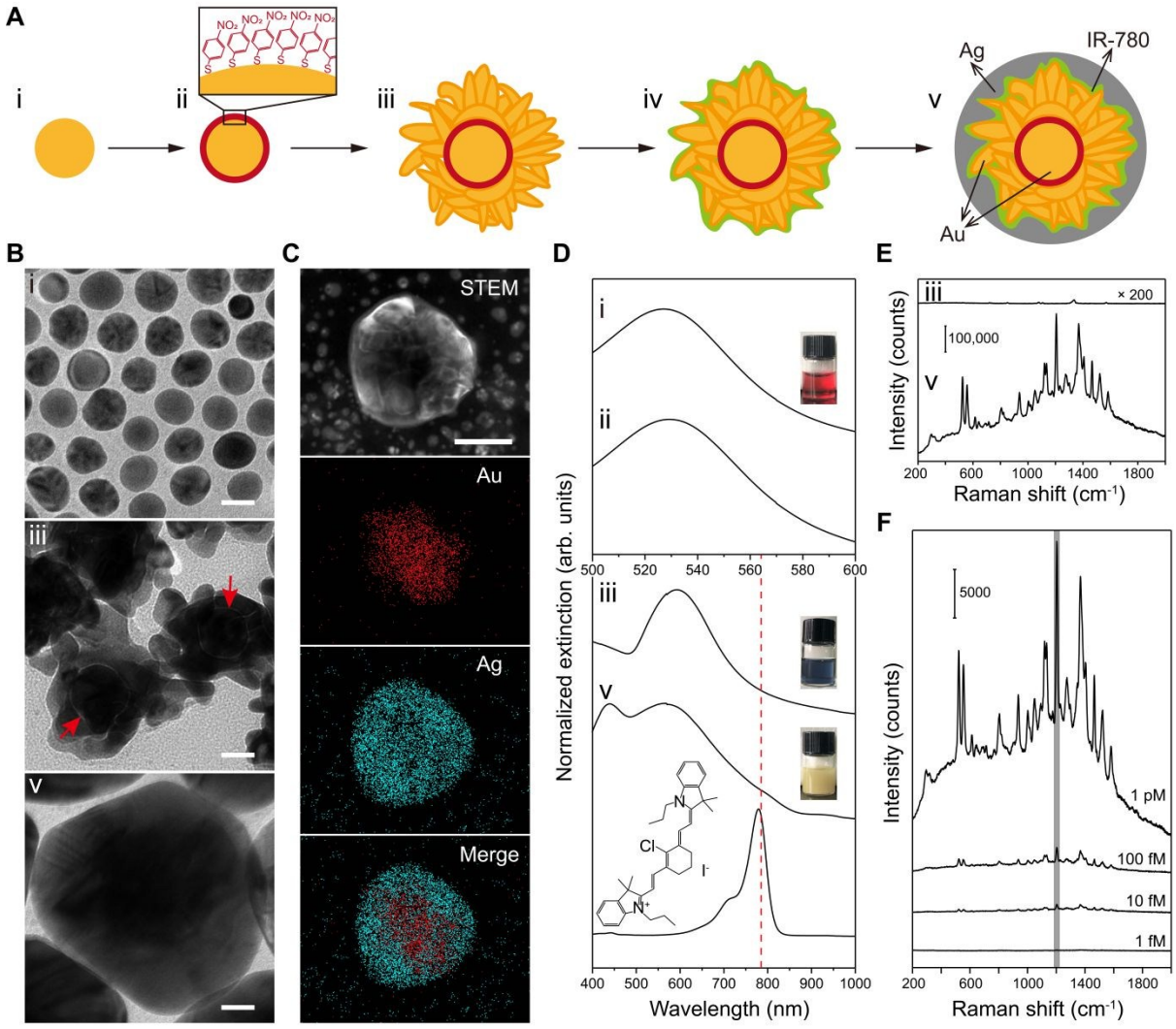

Figure 1. Synthesis and characterizations of gap-enhanced resonance Raman tags (GERRTs). (A) Schematic synthesis process of GERRTs, including (i) Au cores, (ii) 4-nitrobenzenethiol (4-NBT) modified Au cores, (iii) gap-enhanced Raman tags with petal-like shell (P-GERTs), (iv) IR-780 modified P-GERTs and (v) GERRTs. (B) Transmission electron microscopy (TEM) images of the corresponding nanoparticles (NPs) at different synthesis stages. All scale bars are 20 nm. Red arrows indicate the interior nanogaps. (C) The STEM image and the corresponding EDS element mapping images of a GERRT. The scale bar is 50 nm. (D) Extinction spectra of the NPs during the synthesis process and IR-780 iodide (bottom, with the molecular structure). Dashed red line indicates the laser wavelength (785 nm) used in

View Article Online
DOI: 10.1039/D0TB00659A

the Raman measurements. Insets in panel D are the corresponding photos of aqueous NPs. (E) SERS spectra of aqueous (iii) P-GERTs and (v) GERRTs normalized to the laser power (mW). Raman measurements were performed using 785 nm laser, 2 s acquisition time, and ×10 objective lens. (F) Concentration-dependent Raman measurements of aqueous GERRTs (785 nm laser, 29.8 mW, 10 s acquisition time, and ×10 objective lens).

Single-NP detection of GERRTs. Single-NP SERS detection has held great promise to allow high precision diagnosis and ultrasensitive biomedical imaging.[22-24,29,51] Considering the extraordinary SERS activity of GERRTs, we further investigated the single-NP SERS property of GERRTs in the solid state using a correlative Raman imaging and scanning electron microscopy (RISE). The RISE system integrates a stand-alone SEM and a confocal Raman microscope within one instrument. Figure 2A shows the schematic illustration of the measurement process on RISE. To prevent the damage of electron beam to NPs and Raman reporters, single GERRTs on a silicon wafer were first roughly identified under the bright field (Figure 2B) and the corresponding SERS spectra were then collected through the confocal Raman system. After that, the sample was automatically transferred to the SEM chamber to confirm the distribution state of the measured NPs (Figure 2B). To avoid the signals from inter-particle plasmon coupling or multiple NPs in the laser spot, only the data from single GERRTs with a distance of over 1 μm from other NPs was analyzed. After the SEM confirmation, we have successfully performed nine eligible single-GERRT measurements in total, and the corresponding SERS spectra are shown in Figure 2C and Figure S5. It can be seen that the spectra are dominated by three Raman bands at 523, 557 and 1206 cm^{-1}, which agrees with the results in Figure 1E. However, it should be noted that the Raman signal at 523 cm^{-1} may be contributed by the silicon wafer, while the other two bands only belong to IR-780 molecules. We can observe that there exists obvious distinction among the SERS spectra of nine single GERRTs. For instance, three representative particles in Figure 2B exhibit great disparity in Raman

View Article Online
DOI: 10.1039/D0TB00659A

intensity (Figure 2C). Specifically, the intensity at 1206 cm^{-1} is more than 300 counts for particle 3, but only 30 counts for particle 1. In addition, spectral profiles vary a lot among different NPs. For example, the Raman signal at 557 cm^{-1} is stronger than that at 1206 cm^{-1} for particle 3, but the contrary is the case for particle 1. The heterogeneity of the single GERRTs is most probably due to the physisorption of IR-780 molecules onto the NPs, which may lead to different adsorption amounts or orientations of molecules. We believe that it can be improved by some means, e.g., thiol modification,[52] to obtain more stable and homogeneous GERRTs if needed. Overall, most of the single GERRTs turn out to be SERS active, indicating their potentials in ultrasensitive biosensing and bioimaging.

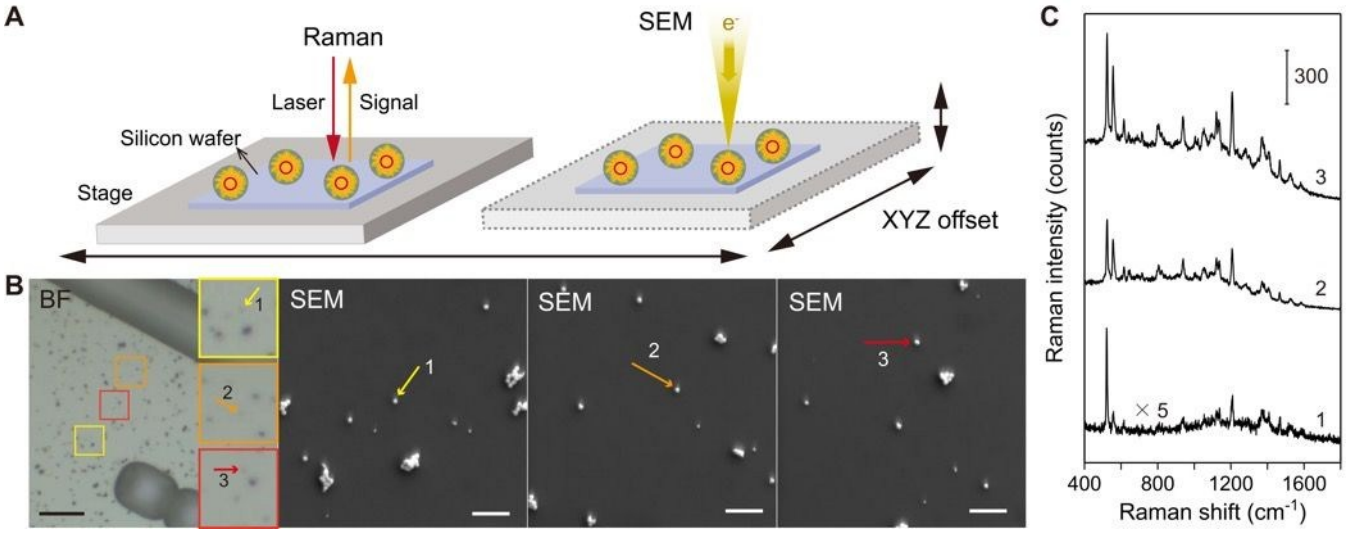

Figure 2. Raman measurements of single GERRTs using the correlative Raman imaging and scanning electron microscopy (RISE). (A) Schematic illustration of the RISE system. (B) A representative bright-field (BF) image of GERRTs on a silicon wafer and the corresponding scanning electron microscopy (SEM) images of three selected single GERRTs (indicated by arrows). Scale bars are 20 μm for the BF image and 1 μm for SEM images. (C) SERS spectra of three single GERRTs (particle 1, 2 and 3) indicated in panel B. Raman measurements were performed using 785 nm laser, 1 mW power, 20 s acquisition time, and ×100 objective lens.

View Article Online
DOI: 10.1039/D0TB00659A

Surface functionalization of GERRTs. In order to minimize the cytotoxicity of Ag and CTAC for better biomedical applications, the GERRTs were coated with biocompatible PDA[31,41] and PEG,[53,54] termed as GERRTs@PDA@PEG (Figure 3A). The PDA layer is acquired by self-polymerization of dopamine under alkaline conditions[41] and can be represented as a collection of oligomeric species formed by the linkage of monomer units through different bondings.[55] The PEGylation is achieved by the covalent bonding between the thiol group in HS-PEG-COOH and the quinone in PDA via the Michael addition reaction.[41] The TEM image of GERRTs@PDA@PEG in Figure 3B shows the uniform surface coating (indicated by a red arrow) with a thickness of approximately 2 nm. After the PDA coating, no significant shift occurs in the extinction spectra (Figure 3C). The average hydrodynamic size of the NPs increases from 147.5 ± 1.0 to 150.6 ± 0.9 nm (Figure 3D), and the zeta potential changes from 59.0 ± 2.5 to 50.8 ± 2.5 mV (Table S1), indicating the successful formation of a thin layer of PDA. After further PEGylation, there is no obvious change for the short-wavelength LSPR peak, but around 30 nm redshift for the longer-wavelength LSPR peak (Figure 3C), which can be explained by the increase of the refractive index of the PEG layer. In addition, the hydrodynamic size of the NPs further increases to 209.8 ± 1.1 nm (Figure 3D), and the zeta potential drops to 10.1 ± 1.7 mV (Table S1), confirming the successful PEG modification. To investigate the cytotoxicity of the surface-functionalized GERRTs, cell viability was determined after Hela cells were treated with GERRTs@PDA@PEG at various concentrations of 0.002, 0.01, 0.05, 0.1 and 0.2 nM for 24 h using a cell counting kit-8 (CCK-8) assay. The results indicate that these nanoprobes demonstrate acceptable low cytotoxicity on Hela cells at concentrations of 0.002, 0.01 and 0.05 nM, but significant cytotoxicity at higher concentrations with cell viabilities below 50% (Figure 3E). It should be noted that bioimaging with these nanoprobes at the

View Article Online
DOI: 10.1039/D0TB00659A

concentration of 0.05 nM is acceptable considering its extraordinarily high SERS activity, as presented in Figure 1E.

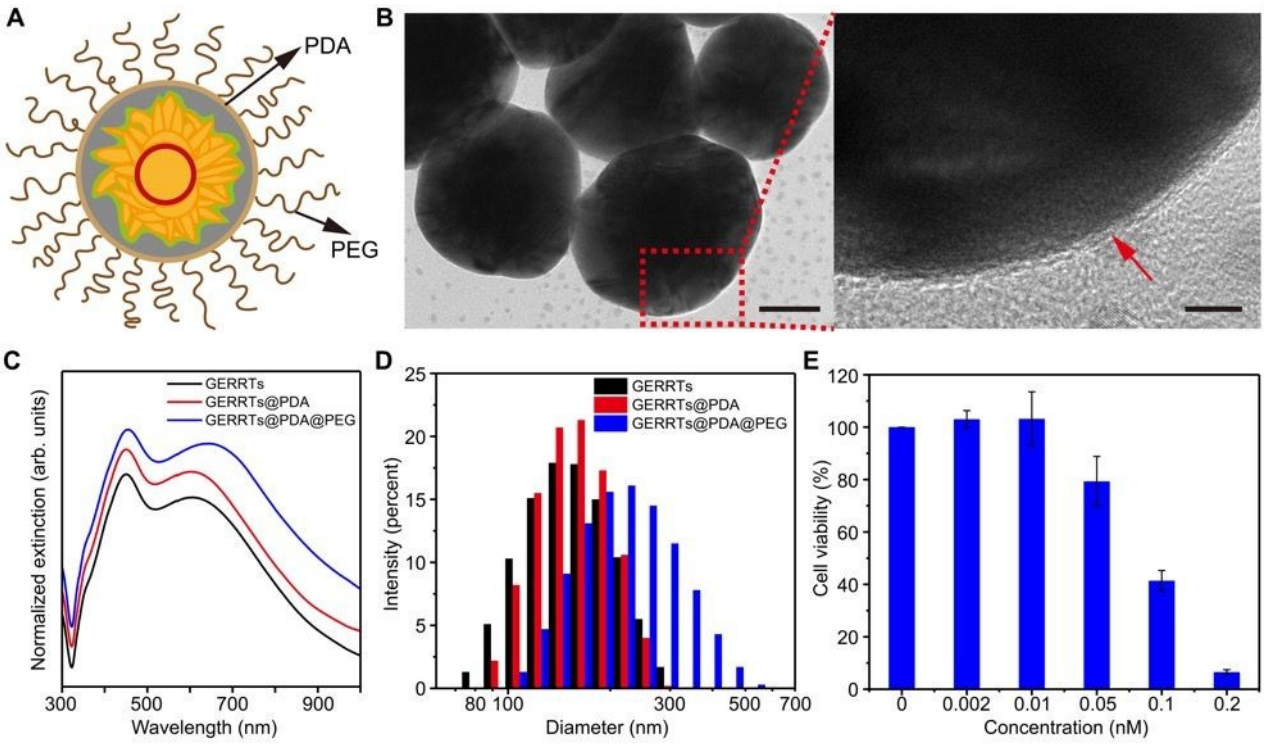

Figure 3. Surface functionalization of GERRTs with polydopamine (PDA) and polyethylene glycol (PEG). (A) Schematic illustration and (B) a TEM image of surface-functionalized GERRTs. Scale bars are 50 nm (left) and 5 nm (right). (C) Extinction spectra and (D) hydrodynamic diameters of GERRTs at different stages of surface functionalization. (E) Cell cytotoxicity evaluation of surface-functionalized GERRTs at different concentrations.

GERRTs for time-lapse live-cell Raman imaging. We then applied the surface-functionalized GERRTs for high-speed live-cell imaging. To provide the cells with suitable biological environment while imaging, we incubated the cells in the UNO STAGE TOP INCUBATOR (Figure 4A) set at 37 °C with 5% CO_2-humidified atmosphere. The incubation system has an air-tight top stage chamber with the controlled internal environment, enabling the long-term survival of live cells. In addition, this type of live-cell system

View Article Online
DOI: 10.1039/D0TB00659A

is integrated with our inverted confocal Raman microscope, which is really in favour of highly efficient live-cell Raman imaging longer for a few days. To track the cellular uptake of NPs via SERS imaging, we refreshed the culture medium of Hela cells with the one containing around 0.05 nM GERRTs after the cells' adhesion to the quartz bottomed plate for 24 h. The concentration of GERRTs was selected according to the cytotoxicity results in Figure 3E. We began to acquire the bright-field image and the corresponding Raman image of the Hela cells 1 h after the NP addition, and thereafter collected the images at an interval of several minutes to observe the entry process of NPs into cells. Figure 4B presents the images of a single cell acquired 2.5 h after the NP addition as an example to show the imaging effect. Herein, we adopted a DuoScan mode along with a SWIFT mode on the confocal Raman system to realize high-speed SERS imaging.[9,56] The Raman mapping image (plotted according to the integrated area of the band at 1206 cm^{-1}, as indicated by the grey area in Figure 4C) in Figure 4B with a scanning area of over 30 × 70 μm^2 and a resolution of 50 × 50 pixels could be accomplished within 12 s with an exposure time of 1 ms per pixel and a laser power of 50 μW. Such high-speed imaging using the ultralow laser power can be attributed to three factors. First, GERRTs can generate ultra-strong Raman signals, thus allowing the reduction of the exposure time down to 1 ms per pixel. Second, the Raman scanning is realized via the rapid movement of the laser spot across the sample controlled by two galvo mirrors instead of the mechanical stage movement. Third, the SWIFT mode allows the line-by-line data processing by detector rather than pixel-by-pixel, thus significantly shortening transmission and processing time of data. Such a short frame acquisition time allows us to record Raman images of cells with a high temporal resolution, and therefore capture dynamic behaviours of live cells. In addition, it is worth noting that the laser power we used in Raman imaging was only 50 μW (a further great reduction compared to our recent work[9]), but Raman signals with sharp and distinct characteristic peaks could still be obtained (e.g., point

View Article Online
DOI: 10.1039/D0TB00659A

3 in Figure 4C). It is expected that the ultralow laser power along with the ultrashort acquisition time of the NIR excitation can significantly reduce the photodamage to live cells, thus enabling long-term viability of cells required in a long period of tracking experiments. Another advantage lies in that the background Raman and autofluorescence signals from cells and the culture dish are negligible with the above-mentioned measurement parameters, consequently resulting in a high-contrast Raman image (Figure 4B).

We can observe from the images in Figure 4B that NPs (the darker part in the bright-field image, confirmed by their SERS spectra, for example, at point 3) gather around the Hela cell 2.5 h after their addition, and may have well interacted with the membrane to enter the cell through endocytosis,[57,58] as indicated by the uneven morphology of the membrane. The Raman image clearly shows that the majority of the cell is void of GERRTs (e.g., point 1), but several scattered bright spots contributed by internalized NPs have appeared inside the cell (e.g., point 2). Figure 5 exhibits the dynamic process of the interaction between NPs and the cell from 1 to 4.5 h after NP addition. It should be noted that some factors including the air/CO_2 piping and heating in the cell culture chamber and the transition of various objective lens may influence the focal plane and accordingly the detected Raman intensity during the imaging. Therefore, the scale bars of Raman intensity at different time points have been adapted to optimize the image visualization.

After cellular uptake, NPs are transported via individual vesicles which will further fuse with endosomes.[57,58] Correspondingly, we can see that bright spots are scattered in the cell exterior during the early stage (1-2.5 h). As time goes on, the internalized NPs gradually move toward the cell interior and eventually reach the perinuclear region (3.75-4.5 h, supported by the bright-field image in Figure 5B), which agrees well with the previous work.[59-61] It has been reported that NPs escaping from vesicular

View Article Online
DOI: 10.1039/D0TB00659A

compartments or trapped in vesicles may enter the nucleus and endoplasmic reticulum, but the mechanisms remain unknown.[57] In addition, we find that the uptake speed of GERRTs by cells is much lower than that of other NPs we reported previously,[9,12] possibly due to the larger size[57,58] of GERRTs and the extra PEGylation which will decrease protein opsonization and consequently cell uptake.[62,63] The Raman images from 3 h 45 min to 4 h 30 min show relatively uneven distributions of Raman intensity around the cell, which can be explained by the inhomogeneous distributions of NPs. The bright-field (BF) image in Figure 5B can further support this, as the brighter areas in the Raman images virtually turn out darker under the BF mode.

Combining EM enhancement and resonance Raman scattering, we have obtained GERRTs with ultrahigh Raman intensity, which not only helps significantly shorten the duration of Raman bioimaging, but also helps reduce the photodamage to biological samples. Minimized exposure energy (determined by both laser power and exposure time) to cells can effectively alleviate the phototoxicity,[64] which without control will influence the viability of living organisms and lead to erroneous conclusions during imaging.[65] In addition, the NIR excitation laser used here is more biologically favorable than short wavelength laser, which tends to cause more serious chemical alteration and breakdown of cellular molecules.[64] Moreover, the GERRTs are under off-resonance excitation as incident laser (785 nm) decouples with the LSPR peak of the NPs, thus producing minimal plasmon-enhanced photothermal effect and perturbation of cells being imaged.[66] Further informative examination of photodamage effect to cells such as monitoring the mitochondrial membrane potential[66] is under investigation.

View Article Online
DOI: 10.1039/D0TB00659A

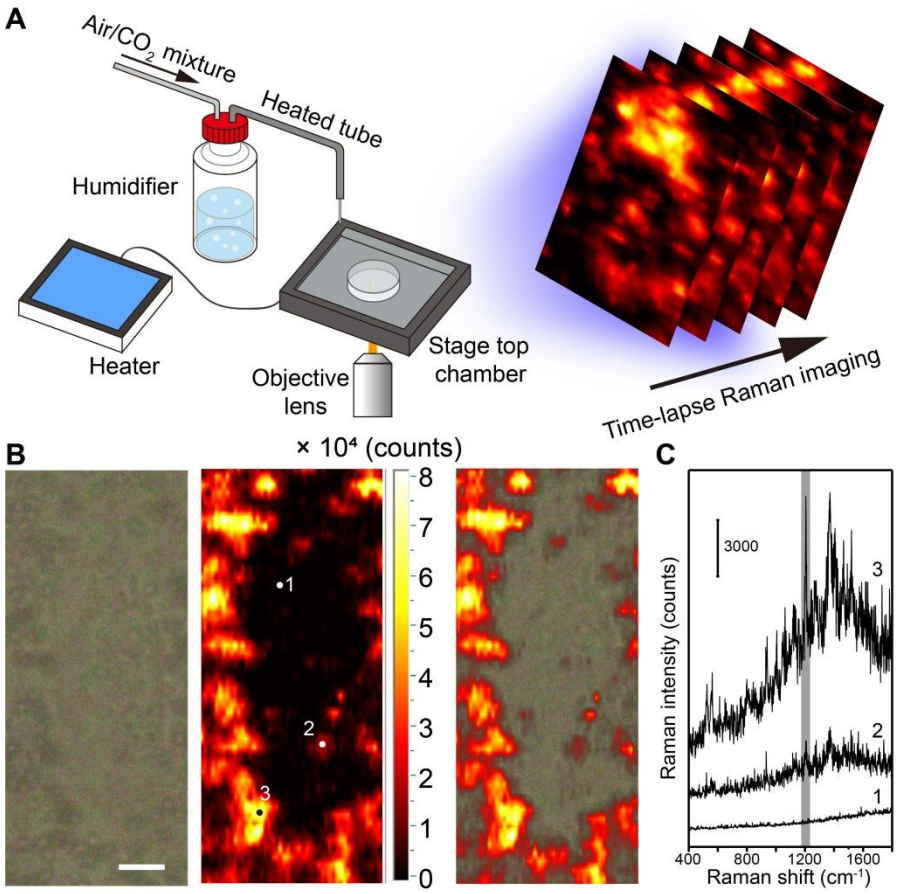

Figure 4. GERRTs for live-cell imaging. (A) Schematic illustration of live cell imaging system (LCS) for time-lapse Raman imaging. (B) BF image (left), Raman image (middle) and the corresponding overlay image (right) of a live Hela cell incubated with GERRTs for 2.5 h. The scale bar is 10 μm. (C) SERS spectra of three points indicated in panel B. The Raman imaging was performed using 785 nm laser, 50 μW power, 1 ms acquisition time, and ×60 objective lens.

View Article Online
DOI: 10.1039/D0TB00659A

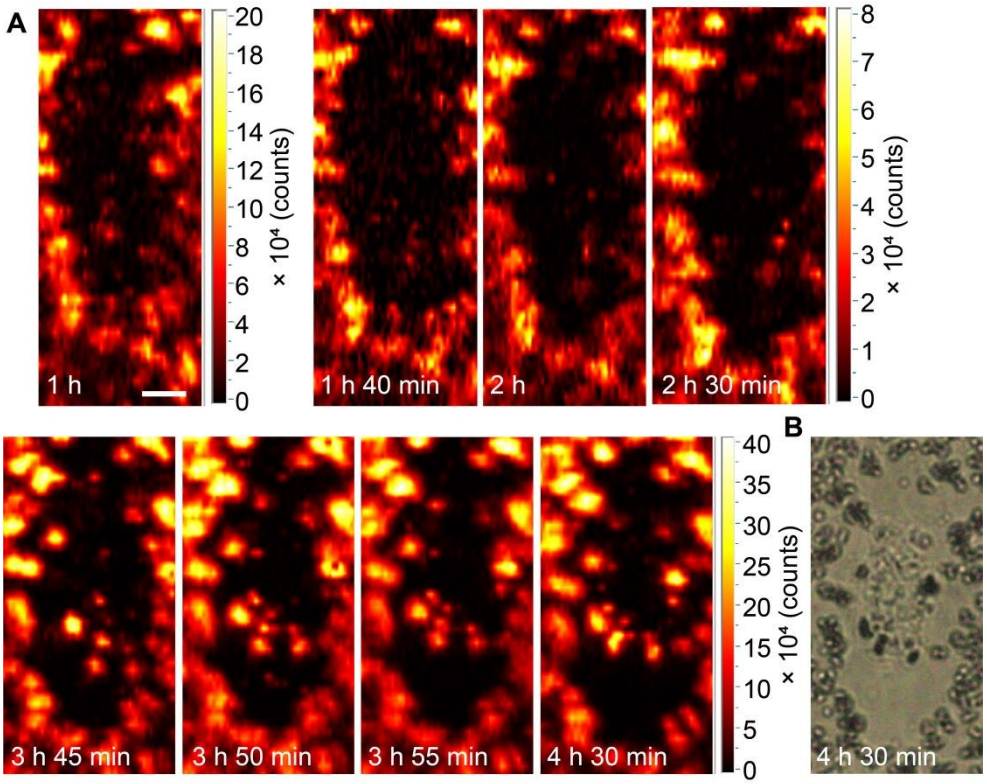

Figure 5. (A) Time-lapse Raman imaging for live Hela cells incubated with GERRTs. The time points represent the incubation durations with NPs. The scale bar is 10 μm. (B) The BF image of the Hela cell after 4.5 h incubation with GERRTs.

Raman imaging for tunneling nanotubes. During one experiment we ran across an unexpected incident: the adhesive quartz bottom of the culture dish became slightly damaged, leading to a very slow leakage of the culture medium (lasting for several hours after the Raman imaging). We found that the cells gradually became unhealthy, as their morphology turned from fusiform to round. Intriguingly, we also observed the formation of many protrusions that connected neighboring cells (Figure 6A), which are termed tunneling nanotubes (TNTs).[67] TNTs are regarded as one of the cell-to-cell communication routes,[67,68] allowing the intercellular transfer of membrane vesicles,[67] organelles,[67] pathogens[69-71] and proteins.[72] According to their diameters, TNTs can be divided into two categories, namely the thinner tubes ($\leqslant$0.7 μm) housing only F-actin and the thicker tubes (>0.7 μm) housing both F-actin and microtubules.[73] Until recently, no clear mechanism has been reported to explain why TNTs form, but

View Article Online
DOI: 10.1039/D0TB00659A

quite a few cases have been related to cells' being subjected to stress, such as addition of reactive oxygen species[74] or serum depletion.[75] It should be noted that we cannot completely exclude the possibility that the NPs also contribute to TNT formation, as they show a very mild cytotoxicity at the concentration of 0.05 nM. However, TNTs were not observed until ~8 h after GERRTs addition, hence indicating that medium depletion was the major cause. Figure 6A demonstrates that the TNTs are visible under the bright field with the diameters over 1 μm. We then selected a part of the TNT region (indicated by a dashed red box) for SERS imaging, as presented in Figure 6B. The Raman image and the corresponding overlay image show that there are NPs inside the TNTs (Figure 6B), which can be confirmed by the obvious Raman bands in the spectra of point 2 and 3 in Figure 6C. The NPs are unlikely located at the outer tube walls in that there are no signals in other regions nearby (e.g., point 1). However, it remains unclear whether the transported NPs are free or trapped in vesicles/endosomes/lysosomes, which requires further investigations.

View Article Online
DOI: 10.1039/D0TB00659A

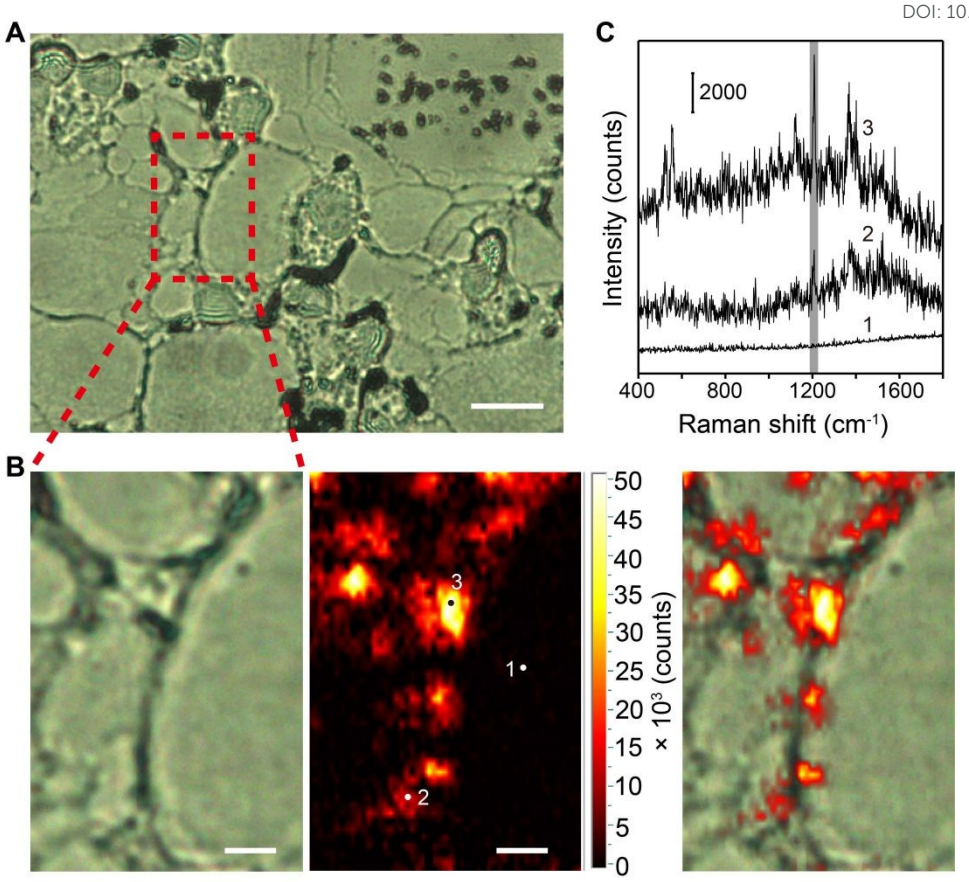

Figure 6. Raman imaging for tunneling nanotubes (TNTs) of Hela cells incubated with GERRTs. (A) BF images of TNTs from Hela cells. The scale bar is 20 μm. (B) Partial magnification of panel A (left), and the corresponding Raman image (middle) and overlay image (right). Scale bars are 5 μm. (C) SERS spectra of three points indicated in the Raman image of panel B.

Conclusion

In summary, we have developed GERRTs with NIR-resonant Raman reporters IR-780 embedded in electromagnetic hot spots from petal-like structure of P-GERTs and plasmon coupling between P-GERTs and Ag shell for high-speed and high-resolution live-cell imaging. GERRTs show approximately three orders of magnitude stronger Raman signals than P-GERTs and a detection limit down to 1 fM of aqueous samples. Raman measurements using the RISE system confirm that single GERRTs in the solid state with obvious Raman characteristic peaks of can be detected. Biofunctionalization of the PDA and PEG layers onto the NPs can further successfully improve their biocompatibility, allowing them suitable for time-

View Article Online
DOI: 10.1039/D0TB00659A

lapse Raman imaging for live Hela cells. Due to the ultrahigh Raman intensity of GERRTs, ultrafast laser scanning technique, and line-by-line data processing method, high-resolution Raman images (50 × 50 pixels) can be accomplished within 12 s with a laser power of 50 μW and exposure time of 1 ms per pixel, which allows the recording of the dynamic process of cells interacting with the NPs. In addition, it is expected that the photodamage to living cells can be dramatically reduced under above-mentioned measuring conditions, which together with the air-tight incubation system can guarantee a long period of cell viability. Herein we have incubated live Hela cells in the stage chamber for more than 8 h and observe that NPs gradually accumulate in the perinuclear region via time-lapse SERS imaging. We also find that NPs can be transported between neighboring cells through TNTs. Overall, GERRTs may open new opportunities for ultrasensitive and low-phototoxic bioimaging to realize long-term tracking of cellular processes.

Conflicts of interest

There are no conflicts of interest to declare.

Acknowledgement

We acknowledge the financial support from the National Natural Science Foundation of China (No. 81871401), the Science and Technology Commission of Shanghai Municipality (No. 19441905300), Innovation Research Plan supported by Shanghai Municipal Education Commission (No. ZXWF082101), Shanghai Jiao Tong University (Nos. YG2017MS54 and YG2019QNA28), Shanghai Key Laboratory of Gynecologic Oncology, and Guangci Professorship Program of Ruijin Hospital.

View Article Online
DOI: 10.1039/D0TB00659A

References

1. Sha, M.Y., Xu, H., Natan, M.J. & Cromer, R. Surface-enhanced Raman scattering tags for rapid and homogeneous detection of circulating tumor cells in the presence of human whole blood. *Journal of the American Chemical Society* **130**, 17214-17215 (2008).
2. Kircher, M.F. et al. A brain tumor molecular imaging strategy using a new triple-modality MRI-photoacoustic-Raman nanoparticle. *Nature medicine* **18**, 829 (2012).
3. Xie, W., Walkenfort, B. & Schlücker, S. Label-free SERS monitoring of chemical reactions catalyzed by small gold nanoparticles using 3D plasmonic superstructures. *Journal of the American Chemical Society* **135**, 1657-1660 (2013).
4. Lane, L.A., Qian, X. & Nie, S. SERS nanoparticles in medicine: from label-free detection to spectroscopic tagging. *Chemical reviews* **115**, 10489-10529 (2015).
5. Su, X. et al. Composite organic− inorganic nanoparticles (COINs) with chemically encoded optical signatures. *Nano letters* **5**, 49-54 (2005).
6. Wang, C., Chen, Y., Wang, T., Ma, Z. & Su, Z. Monodispersed Gold Nanorod-Embedded Silica Particles as Novel Raman Labels for Biosensing. *Advanced Functional Materials* **18**, 355-361 (2008).
7. Zhang, Y. et al. Tunable and linker free nanogaps in core–shell plasmonic nanorods for selective and quantitative detection of circulating tumor cells by SERS. *ACS applied materials & interfaces* **9**, 37597-37605 (2017).
8. Xu, M., Ma, X., Wei, T., Lu, Z.-X. & Ren, B. In situ imaging of live-cell extracellular pH during cell apoptosis with surface-enhanced Raman spectroscopy. *Analytical chemistry* **90**, 13922-13928 (2018).
9. Zhang, Y., Gu, Y., He, J., Thackray, B.D. & Ye, J. Ultrabright gap-enhanced Raman tags for high-speed bioimaging. *Nature communications* **10**, 3905 (2019).
10. Bao, Z. et al. Gap-enhanced Raman tags for high-contrast sentinel lymph node imaging. *Biomaterials* **163**, 105-115 (2018).
11. Qiu, Y. et al. Intraoperative detection and eradication of residual microtumors with gap-enhanced Raman tags. *ACS nano* **12**, 7974-7985 (2018).
12. Zhang, Y. et al. Ultraphotostable mesoporous silica-coated gap-enhanced Raman tags (GERTs) for high-speed bioimaging. *ACS applied materials & interfaces* **9**, 3995-4005 (2017).
13. Kneipp, J., Kneipp, H., Wittig, B. & Kneipp, K. Following the dynamics of pH in endosomes of live cells with SERS nanosensors. *The Journal of Physical Chemistry C* **114**, 7421-7426 (2010).
14. Lin, L. et al. A bioorthogonal Raman reporter strategy for SERS detection of glycans on live cells. *Angewandte Chemie International Edition* **52**, 7266-7271 (2013).
15. Lee, S. et al. Biological imaging of HEK293 cells expressing PLCγ1 using surface-enhanced Raman microscopy. *Analytical chemistry* **79**, 916-922 (2007).
16. Jiang, X. et al. Surface-Enhanced Raman Nanoprobes with Embedded Standards for Quantitative Cholesterol Detection. *Small Methods* **2**, 1800182 (2018).

View Article Online
DOI: 10.1039/D0TB00659A

17. Bálint, S. et al. Diffusion and cellular uptake of drugs in live cells studied with surface-enhanced Raman scattering probes. *Journal of biomedical optics* **15**, 027005 (2010).
18. Kang, B., Austin, L.A. & El-Sayed, M.A. Observing real-time molecular event dynamics of apoptosis in living cancer cells using nuclear-targeted plasmonically enhanced Raman nanoprobes. *ACS nano* **8**, 4883-4892 (2014).
19. Jang, H., Kang, K. & El-Sayed, M.A. Real-time tracking of the autophagy process in living cells using plasmonically enhanced Raman spectroscopy of fucoidan-coated gold nanoparticles. *Journal of Materials Chemistry B* **6**, 5460-5465 (2018).
20. Ando, J., Fujita, K., Smith, N.I. & Kawata, S. Dynamic SERS imaging of cellular transport pathways with endocytosed gold nanoparticles. *Nano letters* **11**, 5344-5348 (2011).
21. Kang, J.W., So, P.T., Dasari, R.R. & Lim, D.-K. High resolution live cell Raman imaging using subcellular organelle-targeting SERS-sensitive gold nanoparticles with highly narrow intra-nanogap. *Nano letters* **15**, 1766-1772 (2015).
22. Harmsen, S. et al. Surface-enhanced resonance Raman scattering nanostars for high-precision cancer imaging. *Science translational medicine* **7**, 271ra277-271ra277 (2015).
23. Huang, R. et al. High precision imaging of microscopic spread of glioblastoma with a targeted ultrasensitive SERRS molecular imaging probe. *Theranostics* **6**, 1075 (2016).
24. Harmsen, S. et al. Rational design of a chalcogenopyrylium-based surface-enhanced resonance Raman scattering nanoprobe with attomolar sensitivity. *Nature communications* **6**, 1-9 (2015).
25. Wang, Y., Yan, B. & Chen, L. SERS tags: novel optical nanoprobes for bioanalysis. *Chemical reviews* **113**, 1391-1428 (2013).
26. Jeanmaire, D.L. & Van Duyne, R.P. Surface Raman spectroelectrochemistry: Part I. Heterocyclic, aromatic, and aliphatic amines adsorbed on the anodized silver electrode. *Journal of electroanalytical chemistry and interfacial electrochemistry* **84**, 1-20 (1977).
27. Albrecht, M.G. & Creighton, J.A. Anomalously intense Raman spectra of pyridine at a silver electrode. *Journal of the american chemical society* **99**, 5215-5217 (1977).
28. Han, L. et al. Surface-Enhanced Resonance Raman Scattering-Guided Brain Tumor Surgery Showing Prognostic Benefit in Rat Models. *ACS applied materials & interfaces* **11**, 15241-15250 (2019).
29. Spaliviero, M. et al. Detection of lymph node metastases with SERRS nanoparticles. *Molecular imaging and biology* **18**, 677-685 (2016).
30. Lim, D.-K. et al. Highly uniform and reproducible surface-enhanced Raman scattering from DNA-tailorable nanoparticles with 1-nm interior gap. *Nature nanotechnology* **6**, 452 (2011).
31. Li, J. et al. A universal strategy for the one-pot synthesis of SERS tags. *Nanoscale* **10**, 8292-8297 (2018).
32. Yuan, H. et al. Quantitative surface-enhanced resonant Raman scattering multiplexing of biocompatible gold nanostars for in vitro and ex vivo detection. *Analytical chemistry* **85**, 208-212 (2013).
33. Zhao, B. et al. Gold nanostructures encoded by non-fluorescent small molecules in polyA-mediated nanogaps as universal SERS nanotags for recognizing various bioactive molecules. *Chemical Science* **5**, 4460-4466 (2014).
34. Ayala-Orozco, C. et al. Fluorescence enhancement of molecules inside a gold nanomatryoshka. *Nano letters* **14**, 2926-2933 (2014).

View Article Online
DOI: 10.1039/D0TB00659A

35. Gandra, N. & Singamaneni, S. Bilayered raman-intense gold nanostructures with hidden tags (brights) for high-resolution bioimaging. *Advanced Materials* **25**, 1022-1027 (2013).
36. Lin, L., Gu, H. & Ye, J. Plasmonic multi-shell nanomatryoshka particles as highly tunable SERS tags with built-in reporters. *Chemical Communications* **51**, 17740-17743 (2015).
37. Khlebtsov, N.G., Lin, L., Khlebtsov, B.N. & Ye, J. Gap-enhanced Raman tags: fabrication, optical properties, and theranostic applications. *Theranostics* **10**, 2067 (2020).
38. Lin, L. et al. Electron Transport Across Plasmonic Molecular Nanogaps Interrogated with Surface-Enhanced Raman Scattering. *ACS nano* **12**, 6492-6503 (2018).
39. Gu, Y. et al. Raman photostability of off-resonant gap-enhanced Raman tags. *RSC advances* **8**, 14434-14444 (2018).
40. Zhang, Y. et al. Intraoperative Raman-Guided Chemo-Photothermal Synergistic Therapy of Advanced Disseminated Ovarian Cancers. *Small* **14**, 1801022 (2018).
41. Zhang, L. et al. A multifunctional platform for tumor angiogenesis-targeted chemo-thermal therapy using polydopamine-coated gold nanorods. *ACS nano* **10**, 10404-10417 (2016).
42. Fales, A.M., Yuan, H. & Vo-Dinh, T. Development of hybrid silver-coated gold nanostars for nonaggregated surface-enhanced Raman scattering. *The Journal of Physical Chemistry C* **118**, 3708-3715 (2014).
43. Jakubowicz, A., Jia, H., Wallace, R. & Gnade, B. Adsorption kinetics of p-nitrobenzenethiol self-assembled monolayers on a gold surface. *Langmuir* **21**, 950-955 (2005).
44. Lin, L., Liu, Z., Li, X., Gu, H. & Ye, J. Quantifying the reflective index of nanometer-thick thiolated molecular layers on nanoparticles. *Nanoscale* **9**, 2213-2218 (2017).
45. Kim, Y., Johnson, R.C., Li, J., Hupp, J.T. & Schatz, G.C. Synthesis, linear extinction, and preliminary resonant hyper-Rayleigh scattering studies of gold-core/silver-shell nanoparticles: comparisons of theory and experiment. *Chemical physics letters* **352**, 421-428 (2002).
46. Varghese, H.T., Panicker, C.Y., Philip, D., Mannekutla, J.R. & Inamdar, S. IR, Raman and SERS studies of methyl salicylate. *Spectrochimica Acta Part A: Molecular and Biomolecular Spectroscopy* **66**, 959-963 (2007).
47. Perna, G., Lasalvia, M., Gallo, C., Quartucci, G. & Capozzi, V. Vibrational characterization of synthetic eumelanin by means of Raman and surface enhanced Raman scattering. *The Open Surface Science Journal* **5** (2013).
48. Razmutė, I., Kuodis, Z., Eicher-Lorka, O. & Niaura, G. Surface-enhanced Raman spectroscopy of indole ring-terminated self-assembled monolayer on silver electrode. *Chemija* **17** (2006).
49. Doering, W.E. & Nie, S. Single-molecule and single-nanoparticle SERS: examining the roles of surface active sites and chemical enhancement. *The Journal of Physical Chemistry B* **106**, 311-317 (2002).
50. Kneipp, K. et al. Single molecule detection using surface-enhanced Raman scattering (SERS). *Physical review letters* **78**, 1667 (1997).
51. Li, L., Hutter, T., Steiner, U. & Mahajan, S. Single molecule SERS and detection of biomolecules with a single gold nanoparticle on a mirror junction. *Analyst* **138**, 4574-4578 (2013).
52. Zhang, Y. et al. Enhancing sensitivity of SERRS nanoprobes by modifying heptamethine cyanine-based reporter molecules. *Journal of Innovative Optical Health Sciences* **9**, 1642005 (2016).
53. Zhang, M., Li, X., Gong, Y., Zhao, N. & Zhang, X. Properties and biocompatibility of chitosan films modified by blending with PEG. *Biomaterials* **23**, 2641-2648 (2002).

View Article Online
DOI: 10.1039/D0TB00659A

54. Wu, H. et al. Biocompatibility, MR imaging and targeted drug delivery of a rattle-type magnetic mesoporous silica nanosphere system conjugated with PEG and cancer-cell-specific ligands. *Journal of Materials Chemistry* **21**, 3037-3045 (2011).
55. Della Vecchia, N.F. et al. Building-block diversity in polydopamine underpins a multifunctional eumelanin-type platform tunable through a quinone control point. *Advanced Functional Materials* **23**, 1331-1340 (2013).
56. Gu, Y. et al. Gap-enhanced Raman tags for physically unclonable anticounterfeiting labels. *Nature Communications* **11**, 516 (2020).
57. Behzadi, S. et al. Cellular uptake of nanoparticles: journey inside the cell. *Chemical Society Reviews* **46**, 4218-4244 (2017).
58. Mosquera, J.s., García, I. & Liz-Marzán, L.M. Cellular uptake of nanoparticles versus small molecules: A matter of size. *Accounts of chemical research* **51**, 2305-2313 (2018).
59. Shah, N.B., Dong, J. & Bischof, J.C. Cellular uptake and nanoscale localization of gold nanoparticles in cancer using label-free confocal Raman microscopy. *Molecular pharmaceutics* **8**, 176-184 (2011).
60. Lamprecht, C. et al. Mapping the intracellular distribution of carbon nanotubes after targeted delivery to carcinoma cells using confocal Raman imaging as a label-free technique. *Journal of Physics: Condensed Matter* **24**, 164206 (2012).
61. Ahlinder, L., Ekstrand-Hammarström, B., Geladi, P. & Österlund, L. Large uptake of titania and iron oxide nanoparticles in the nucleus of lung epithelial cells as measured by Raman imaging and multivariate classification. *Biophysical journal* **105**, 310-319 (2013).
62. Li, Y., Kröger, M. & Liu, W.K. Endocytosis of PEGylated nanoparticles accompanied by structural and free energy changes of the grafted polyethylene glycol. *Biomaterials* **35**, 8467-8478 (2014).
63. Van Haute, D., Liu, A.T. & Berlin, J.M. Coating metal nanoparticle surfaces with small organic molecules can reduce nonspecific cell uptake. *ACS nano* **12**, 117-127 (2018).
64. Laissue, P.P., Alghamdi, R.A., Tomancak, P., Reynaud, E.G. & Shroff, H. Assessing phototoxicity in live fluorescence imaging. *Nature methods* **14**, 657-661 (2017).
65. Magidson, V. & Khodjakov, A. Circumventing photodamage in live-cell microscopy. *Methods in Cell Biology* **114**, 545-560 (2013).
66. Jin, X., Khlebtsov, B.N., Khanadeev, V.A., Khlebtsov, N.G. & Ye, J. Rational design of ultrabright SERS probes with embedded reporters for bioimaging and photothermal therapy. *ACS applied materials & interfaces* **9**, 30387-30397 (2017).
67. Rustom, A., Saffrich, R., Markovic, I., Walther, P. & Gerdes, H.-H. Nanotubular highways for intercellular organelle transport. *Science* **303**, 1007-1010 (2004).
68. Gerdes, H.-H. & Carvalho, R.N. Intercellular transfer mediated by tunneling nanotubes. *Current opinion in cell biology* **20**, 470-475 (2008).
69. Önfelt, B. et al. Structurally distinct membrane nanotubes between human macrophages support long-distance vesicular traffic or surfing of bacteria. *The Journal of Immunology* **177**, 8476-8483 (2006).
70. Gousset, K. et al. Prions hijack tunnelling nanotubes for intercellular spread. *Nature cell biology* **11**, 328-336 (2009).
71. Sherer, N.M. & Mothes, W. Cytonemes and tunneling nanotubules in cell–cell communication

View Article Online
DOI: 10.1039/D0TB00659A

and viral pathogenesis. *Trends in cell biology* **18**, 414-420 (2008).

72. Epperla, C.P., Mohan, N., Chang, C.W., Chen, C.C. & Chang, H.C. Nanodiamond-Mediated Intercellular Transport of Proteins through Membrane Tunneling Nanotubes. *Small* **11**, 6097-6105 (2015).
73. McGOWAN, M. Tunneling nanotubes-Crossing the bridge. *Journal of Cell & Molecular Biology* **9** (2011).
74. Zhu, D. et al. Hydrogen peroxide alters membrane and cytoskeleton properties and increases intercellular connections in astrocytes. *Journal of cell science* **118**, 3695-3703 (2005).
75. Wang, Y., Cui, J., Sun, X. & Zhang, Y. Tunneling-nanotube development in astrocytes depends on p53 activation. *Cell Death & Differentiation* **18**, 732-742 (2011).